Journal of Power Sources 558 (2023) 232546

Contents lists available at ScienceDirect

Journal of Power Sources

journal homepage: www.elsevier.com/locate/jpowsour

Alternative solvents for Lithium-Nickel-Cobalt-Manganese-Oxide electrode fabrication for lithium-ion-cells

Fabian Heim [a,*], Frauke Langer [b,c], Anja Paulus [b], Tina Kreher [a], Peter Birke [a]

[a] Electrical Energy Storage Systems, Institute for Photovoltaics, University of Stuttgart, Germany
[b] Mercedes-Benz Group AG, Stuttgart, Germany
[c] Chemistry of Thin Film Materials, IZNF, Friedrich-Alexander University of Erlangen-Nürnberg, Germany

HIGHLIGHTS

- Alternative solvents for PVDF binder in NCM electrodes exist.
- Cathodes that are processed with alternative solvents do not show major drawbacks.
- The use of different binder solvents affects the drying behavior.
- GDOES was used to determine carbon distribution along the height of NCM electrodes.

ARTICLE INFO

Keywords:
Cathode
NCM
NMC
NMP
NMP-free
DMSO
TEP
GDOES
Carbon distribution

ABSTRACT

In this paper we investigate alternative solvents for dissolving Polyvinylidene fluoride (PVDF) to substitute harmful N-Methyl-2-pyrrolidone (NMP) in the manufacturing process of Lithium-Nickel-Cobalt-Manganese-Oxide (NCM) electrodes. Therefore NCM cathodes are prepared using Dimethyl sulfoxide (DMSO) and Triethyl phosphate (TEP) based slurries. With these electrodes cells against graphite anodes are set up and tested in three ways: Current pulses, discharge current rate and cyclic aging. The comparison of the test results with conventionally NMP-processed electrodes indicate that the substitution of NMP by DMSO or TEP does not involve any serious drawbacks.

1. Introduction

The current state-of-the-art manufacturing process for positive electrodes of lithium-ion-batteries requires the use of volatile and harmful N-Methyl-2-pyrrolidone (NMP) [1]. Since the use of NMP is strongly regulated in the Annex XVII to the REACH regulation [2] the search for alternative manufacturing routes is a current issue.

One method to avoid the use of NMP is dry coating of active material onto current collectors as in [3]. So far this method has not been adopted in industrial production.

Bresser et al. [4] reviewed the current state of research concerning binders and solvents for batteries. For negative electrodes the aqueous processable binder styrene butadiene rubber in combination with the water soluble thickening agent sodium carboxymethyl cellulose (Na-CMC) has been state-of-the-art for many years [5]. For lithium transition metal oxide based positive electrodes no equivalent alternatives to NMP were established yet. Promising results with aqueous binders for cathodes were shown in [6,7]. However their commercialization was not accomplished till today.

In [8,9] different suitable solvents for PVdF have been investigated. Among them DMSO and TEP which do not have a classification as potentially carcinogenic or toxic to reproduction within the Globally Harmonized System of Classification (GHS).

To the best of our knowledge Dimethyl sulfoxide (DMSO) was first shown to be a possible replacement candidate for NMP by [10]. The properties of their electrodes manufactured with DMSO were very similar to conventional electrodes manufactured with NMP as solvent. In addition to the results presented in the addressed publication we demonstrate the feasibility of TEP as solvent.

As far as we know Triethyl phosphate (TEP) was first mentioned as solvent of binders for electrode slurries in [11]. In [12] Chang et al. use TEP as solvent to produce PVdF membranes for membrane distillation.

* Corresponding author.
E-mail address: fabian.heim@ipv.uni-stuttgart.de (F. Heim).

https://doi.org/10.1016/j.jpowsour.2022.232546
Received 9 July 2022; Received in revised form 2 December 2022; Accepted 17 December 2022
Available online 5 January 2023
0378-7753/© 2022 Published by Elsevier B.V.

LGES 1062
LGES v. MRD
IPR2024-01013

In this communication we would like to demonstrate the comparison of two alternatives to NMP that can be used to dissolve fluorinated polymers and together act as binder solutions for electrode slurries.

2. Experimental

2.1. Electrode preparation

The active material of the positive electrodes is $LiNi_{0,6}Co_{0,2}Mn_{0,2}O_2$ (NCM-622, 178 mAh/g, Basf Hed Ncm). Imerys C-Nergy Super C65 is employed as conductive additive. The homopolymer Polyvinylidene fluoride (PVdF, in 10% solution, Sigma-Aldrich, M_w = 530,000) is used as the binder. For reference electrodes N-Methyl-2-pyrrolidone (NMP, Carl-Roth GmbH, 99.8%) acts as the solvent. The solvents Dimethyl sulfoxide (DMSO, Carl Roth GmbH, 99.8%) and Triethyl phosphate (TEP, Sigma-Aldrich, 99.8%) serve as replacement for NMP in the alternative electrode slurries. Before use all solvents are dried with the help of molecular sieves with a pore size of 3 Å.

The composition of all positive electrodes is 96 wt.% active material, 2 wt.% conductive additive and 2 wt.% binder. The total mass of the solids of cathode slurries is 100 g, the mass of solvent for NMP-based slurries is 42.86 g (70 wt.% solid content). To adjust the viscosity of the alternative electrode slurries to the value of the NMP-based one their solid content is reduced to 67.5 wt.% (100 g solids, 48.15 g solvent).

Negative electrodes consist of 96 wt.% graphite (Imerys Timrex Sls30) and 1 wt.% conductive additive (Super C65). For the binder 1.5 wt.% Sodium Carboxymethylcellulose (Na-CMC, in 4% aqueous solution, Sigma-Aldrich, M_w = 250,000, DoS = 1.2) and 1.5 wt.% styrene-butadiene rubber in aqueous emulsion (SBR, Lipaton, 50%) are used. The total mass of solids of anode slurries is 30 g, the mass of water is 33.16 g (47.5% solid content).

All components are mixed in a planetary mixer (Thinky Are-250) in 150 mL containers including 20 g ceramic balls with a diameter of 5 mm to accelerate deagglomeration. The active material and the conductive additive are premixed without solvent (but with ZrO_2 balls) for 60 min at 300 rpm in order to favor the formation of a thin carbon-layer on the surface of the active material particles. After adding half of the total solvent, the slurry is mixed at high viscosity at 2000 rpm for 1 min to break down remaining agglomerates. After adding the remaining half of the total solvent, the slurry is mixed three times for one minute at 2000 rpm with cool down periods in between. Just before the coating, slurries are mixed for 20 s at 300 rpm to prevent and counter sedimentation and centrifugal force during mixing at higher speed. Positive electrodes are coated onto aluminum foil (30 μm thickness), for negative electrodes copper foil (20 μm thickness) is used. The coating is done with the application device Zehntner Zaa 2300 and the doctor blade Zehntner Zua 2000.

The specific capacity of the positive electrode is set to $C_+ = 3\,\mathrm{mAh/cm^2}$ (corresponding to a loading of 16.85 g/cm^2 active material) and the ratio of the negative to positive electrode's capacity (N/P-ratio) is 1.1 (determined before cell formation). Only for current rate and cycle aging tests two different electrode loadings are investigated ($C_+ = 2\,\mathrm{mAh/cm^2}$ and $C_+ = 3\,\mathrm{mAh/cm^2}$, N/P-ratio = 1.1).

Evaporation of solvent after coating is accomplished on a hot plate under a fume hood at 120 °C for half an hour. Positive electrodes are compacted with a hydraulic press (Specac GS15011) and a pressing die (Paul-Otto Weber GmbH) to a porosity of about 35%. Negative electrodes are compacted to about 40% porosity. Porosity is calculated by the formula:

$$\Phi = \frac{V_t - V_s}{V_s} \tag{1}$$

where V_t is the total volume of the porous electrode, determined by its height and base area, and V_s is the volume of the electrode's solid particles, determined by the particle's mass and density. The inaccuracy of porosity determination (about ±1%) is mainly owed to deviations in the measurement of the electrode's thickness.

To remove moisture and traces of solvent electrodes are dried in a vacuum oven (Büchi B-585) at 120 °C for 16 h.

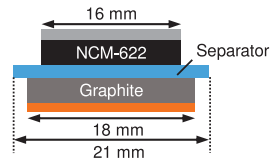

Fig. 1. Schematic drawing of coincell construction. Misalignment of the round electrodes is prevented by a geometric overhang of negative electrodes.

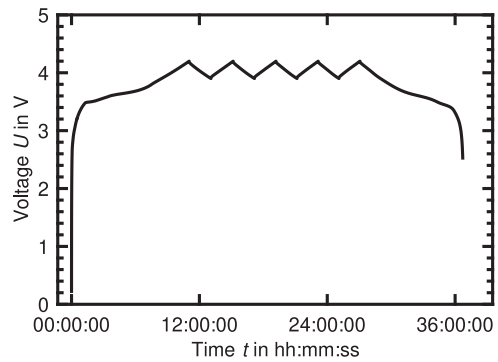

Fig. 2. Voltage during accelerated electrode formation: One single cycle is carried out at C/10. 4 micro-cycles are included between 3.9 and 4.2 V.

2.2. Cell preparation

Cells are built in an Argon filled glove-box (MBraun). Freudenberg FS2190 with a thickness of 170 μm is used as separator and soaked with 100 μL of electrolyte (1 M $LiPF_6$ in ethylene carbonate and diethyl carbonate (1:1 (wt.))).

2.2.1. Lithium reference electrode tests

EL-Cells Pat-Cell system with a lithium-metal-ring-electrode is used for reference electrode measurements. Therefore the NCM electrodes are manufactured with a specific capacity of $C_+ = 3\,\mathrm{mAh/cm^2}$ and a diameter of 18 mm and graphite electrodes with $C_- = 3.3\,\mathrm{mAh/cm^2}$ and a diameter of 18 mm.

2.2.2. Current pulse, current rate and cycle aging tests

Current pulse, current rate and cycle aging tests are performed in CR2325 coincells. In [13] it is demonstrated how geometric misalignment of electrodes can negatively influence the cycling behavior of full cells. Coincells lack the insulation sleeve, which is of great help during vertical alignment of the two electrodes. Thus to prevent electrode misalignment, negative electrodes for rate, cycle aging and pulse characterization tests are manufactured with a geometric overhang as shown in Fig. 1. Positive electrodes are punched to round disks with a diameter of 16 mm while for negative electrodes a diameter of 18 mm is chosen.

2.3. Cell formation and electrochemical characterization

All tests are conducted in climate chambers (Memmert) at 25 °C using the test system Cts by Basytec. The cell formation takes place according to a protocol for "accelerated formation" proposed by [14]. The associated voltage curve is shown in Fig. 2 and consists of one single charge and discharge cycle at a C-rate of C/10 including 4 micro-cycles at high state of charge (SoC) between 4.2 and 3.9 V.

For current rate discharge tests cells are first charged at C/2 followed by a constant voltage phase at 4.2 V until the current drops below C/10. Cells are discharged twice at rates of 1 C, 2 C, 3 C and 4 C to a voltage of 2.5 V. Afterwards, 100 aging cycles at a 1 C charge and discharge rate with voltage limits of 2.5 and 4.2 V are conducted.

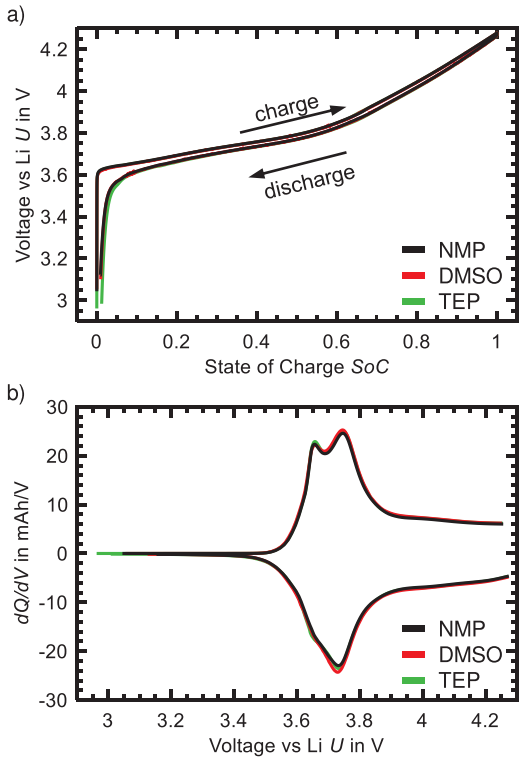

Fig. 3. (a) Potentials of the differently manufactured NCM electrodes (3.0 mAh/cm^2) captured in full cells against graphite (3.3 mAh/cm^2) measured against a lithium-ring-reference-electrode after formation. (b) Differential capacities as a function of potentials vs. Li of the differently manufactured NCM622 electrodes. (For interpretation of the references to color in this figure legend, the reader is referred to the web version of this article.)

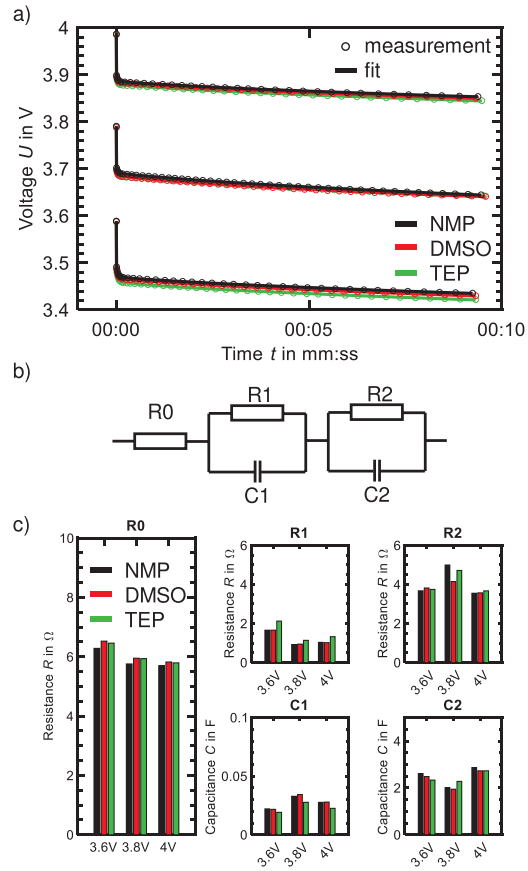

Fig. 4. (a) Current pulse measurements with a rate of 2 C over 10 s on cells with NCM622 electrodes (3.0 mAh/cm^2) against graphite (3.3 mAh/cm^2) at cell voltages of 3.6, 3.8 and 4.0 V. Circles depict the measured voltages and lines represent the voltage curves generated by fitting a second order Thevenin model (b). (c) Diagram of the parameters that were determined using the equivalent circuit model. (For interpretation of the references to color in this figure legend, the reader is referred to the web version of this article.)

A constant voltage phase at 4.2 V during which the charge current is reduced to C/10 is included.

Pulse tests are performed at different SoCs which are defined by the cells open circuit voltage (OCV = 3.6, 3.8 and 4 V). Those SoCs are set by charging at a rate of C/2 up to the desired voltage and reducing the current to a rate of C/10. Pulses of 2 C are conducted after a pause of 1 h for 10 s.

2.3.1. GDOES measurements

Glow-discharge optical emission spectroscopy (GDOES) measurements are performed with a GDA750 spectrometer (Spectruma) with an air-excluding chamber. Argon gas is employed as discharging gas. The analyzed spot size is 2.4 mm in diameter. Radio frequency power and pulsed glow discharge were applied with 600 V and 200 Pa gas pressure. The emission line 165,70 nm is used for carbon detection.

3. Results and discussion

3.1. Comparison of voltage curves vs. Li-reference

Fig. 3(a) shows potential curves vs. Li of the differently manufactured NCM electrodes after formation. Here 0% SoC respectively 100% SoC is defined by a voltage of 2.5 V respectively 4.2 V of the full cell (vs. graphite) at a current rate of C/10. The black line shows the curve of the electrode produced with NMP. The graphs with alternative solvents (red = DMSO and green = TEP) indicate a very similar behavior. No significant difference can be seen.

For further analysis the measurements mentioned above are shown in a dQ/dU vs. U diagram (Fig. 3(b)). This way differences of the OCVs can be displayed more clearly. Due to noise in the voltage measurement smoothing was necessary before differentiating. In accordance to literature [15,16] the curves with peaks during charge at about 3.65 V and 3.75 V and one single peak at about 3.72 V during discharge are as expected for NCM622 cathode material. As in Fig. 3(a), the curves of the three electrodes prepared with different solvents lie almost exactly on top of each other. The small deviations in the area of the peaks can be justified with tolerances during production. Based on these measurements, it can be assumed that processing of NCM with different solvents does not affect the electrochemical properties of the finished electrodes. Furthermore, there is no difference between the two alternatives DMSO and TEP.

3.2. Current pulse measurements

To investigate possible effects of the solvents on the internal resistance of the cells and the dynamic behavior, current pulses are applied to cells containing the differently manufactured electrodes. In Fig. 4(a) the measured voltage responses of full cells to current pulses of 2 C over a duration of 10 s at open circuit potentials of 3.6, 3.8 and 4.0 V are shown. The curves of cell voltages of the NCM electrodes fabricated with DMSO (red) and TEP (green) are almost congruent with the NMP reference cell (black).

For detailed analysis a basic second-order Thevenin model 4(b) to represent ohmic resistance (R0) double layer (C1 and C2) and charge transfer (R1 and R2) effects at surfaces of the electrodes [17] was fit to the data and parameters are shown in Fig. 4(c). If the values of the NMP reference cell for the ohmic resistance R0 are compared with

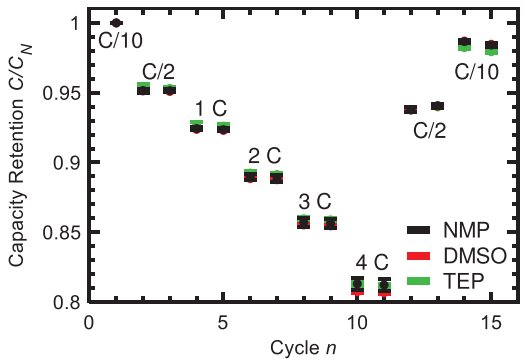

Fig. 5. Rate test of cells with different binder-solvents for positive electrodes and a specific capacity of 2 mAh/cm^2. Each marker with error bar represents the mean value of discharge capacity of two cells while the displayed values are all normalized to the discharge capacity of the first shown cycle at C/10.

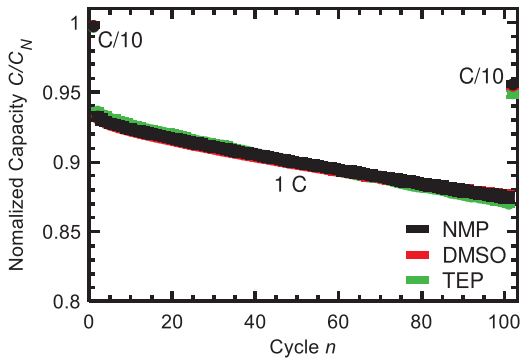

Fig. 6. Cycle test of cells with different binder-solvents for positive electrodes and a specific capacity of 2 mAh/cm^2. Each marker with error bar represents the mean value of discharge capacity of two cells while the displayed values are all normalized to the discharge capacity of the first shown cycle at C/10. For better visibility only every third cycle is shown.

the two alternatives, they are only minimally higher. However, the difference can be attributed to measurement inaccuracies and marginal manufacturing differences.

The similarity of the shown parameters imply that the herein investigated different binder solvents do not influence the properties and dynamic behavior of the therewith manufactured cathodes.

3.3. Rate capability and cycle aging

In Fig. 5 the results of rate capability tests of cells with 2 mAh/cm^2 are displayed.

The markers with error bars represent the mean value of the discharge capacity of two cells each while the values are normalized to the first capacity measured at a rate of C/10. At a C-rate of 4, the cells with DMSO processed cathodes, show slightly reduced discharge capacity compared to the other two systems (DMSO: 80.7% of capacity retention, NMP & TEP: 81.3% of capacity retention). The other C-rates do not show any major deviation in discharge capacity. However at the last both cycles at a rate of C/10 the discharge capacities of the TEP cells (98.2%) is noticeably smaller when compared to the NMP and DMSO (98.7%) system. We ascribe this minor deviations to manufacturing tolerances.

Fig. 6 shows the results of the cycle test that is conducted with the same cells and directly subsequent to the rate capability test.

Again, mean values with error bars of two cells each with normalization to the first cycle at C/10 are shown. After 100 cycles at a rate of 1 C, the capacity check at a rate of C/10 yields a value of

Table 1
Porosities of electrodes before compression and required compaction pressure to obtain the desired porosity.

System	Un-compressed	Pressure in MPa to yield 35% porosity
NMP	55%	100
DMSO	60%	125
TEP	74%	175

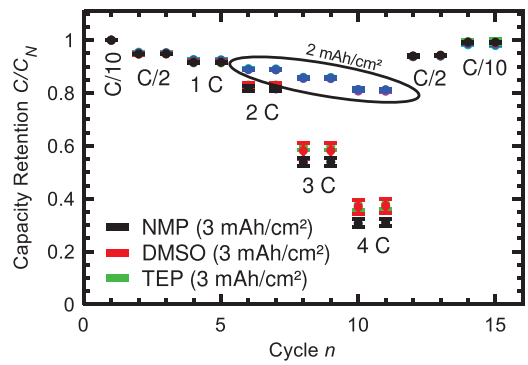

Fig. 7. Rate test of cells with different binder-solvents for positive electrodes and a specific capacity of 3 mAh/cm^2. Each marker with error bar represents the mean value of discharge capacity of two cells while the displayed values are all normalized to the discharge capacity of the first shown cycle at C/10. For direct comparison the results of cells with a loading of 2 mAh/cm^2 from Fig. 5 are displayed in blue. (For interpretation of the references to color in this figure legend, the reader is referred to the web version of this article.)

95.6% for the NMP-system, 95.5% for the DMSO-system and 94.9% for the TEP system. Among others a possible explanation might be small differences in the manufacturing process. Slurries for DMSO and TEP electrodes require a higher amount of solvent (32.5% compared to 30%) in order to gain comparable viscosity for a homogeneous coating than with the NMP system. The coating of slurries with a higher proportion of solvent results in a more porous electrode, and requires higher pressures during compaction to yield the same porosity as shown in Table 1. As stated in the experimental part especially the determination of the electrode's porosities is prone to minor inaccuracy. In [18] it was shown that the anode's porosity has influence on the aging behavior of lithium-ion cells. If we assume that this context is transferable to positive electrodes, slightly different porosities of the NMP, DMSO and TEP systems might be an explanation for the different capacity retentions. Another possible reason, that is still to be examined, is the contamination of the electrodes with residual solvent or decomposition products thereof. Furthermore in all results of full-cell tests slight manufacturing tolerances of the negative electrodes cannot be ignored.

With a trend to high energy lithium-ion cells with specific electrode capacities we also investigated DMSO and TEP for cathode manufacturing with a loading of 3 mAh/cm^2. In Fig. 7 rate capability tests of those cells are shown.

Compared to the results of cells with a specific capacity of 2 mAh/cm^2 as in Fig. 6 it can be noticed that the accessible charge amount decreases distinctly with increasing discharge rates. This behavior can be observed for all the differently manufactured electrodes and a possible explanation might be the following: Rate capability of thick electrodes has been investigated by [3]. They also observed significant decrease in discharge capacity with increasing electrode thickness and ascribed the behavior to transport limitations dominated by longer diffusion paths through the electrolyte-phase of the porous electrodes. Morasch et al. [19] looked into performance limiting factors in graphite electrodes in more detail. Among electrodes with different loadings (0.6, 1.5, 2.9 an 7.5 mAh/cm^2) they identified those with

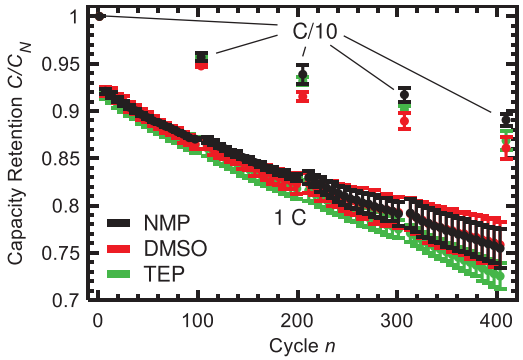

Fig. 8. Cycle test of cells with different binder-solvents for positive electrodes and a specific capacity of 3 mAh/cm^2. Each marker with error bar represents the mean value of discharge capacity of three cells while the displayed values are all normalized to the discharge capacity of the first shown cycle at C/10. For better visibility only every sixth cycle is shown.

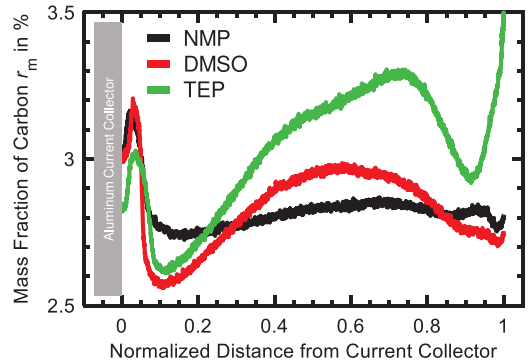

Fig. 9. Distribution of carbon along the depths from the current collector to the surface of the three differently manufactured cathodes determined by GDOES measurements. The apparent maxima on the surface of the electrodes (at a distance of 1 from the current collector) result from measurement artifacts.

a specific capacity of 2.9 mAh/cm^2 and 7.5 mAh/cm^2 as those with predominantly transport limiting properties (in opposite to thinner electrodes that are rather kinetically limited). One may assume that the herein investigated electrodes with specific capacities of 2 mAh/cm^2 rather fall into the category of kinetically limited ones while the electrodes with 3 mAh/cm^2 are rather transport limited. Another fact that has to be considered when looking at the weak high current performance of thicker electrodes is that at constant C-rates current densities (with respect to the area of the electrode/separator interface) rise proportional with increasing area specific capacity.

An explanation for the deviation between cells with different binder solvent at rates of 3 and 4 C might be the already mentioned slight differences in microstructure due to the manufacturing of electrodes with different solid contents of the slurry.

In Fig. 8 the same cells underwent an extensive cyclic aging at charge and discharge current rates of 1 C with capacity checks at a current rate of 1/10 C each after 100 cycles.

Despite the similarity of the capacity retention curves it is obvious, especially when looking at the 1/10 C cycles that the NMP manufactured electrodes show the most stable behavior. TEP manufactured electrodes have higher capacity decay in both high (1 C) and low current (1/10 C) discharge cycles. DMSO manufactured electrodes however have comparable capacity retention in high current discharge cycles but show the highest capacity decay at low current rates (Table 2).

One possible reason for this behavior was identified by GDOES measurements. Fig. 9 shows the mass fraction of carbon as a function of distance from the current collector for the 3 differently manufactured cathodes. For better comparison the x-axis is normalized. The carbon containing components of the investigated cathodes are the conductive additive (2 wt.-% carbon among all solid contents) and PVdF-binder (0.75 wt.-% carbon among all solid contents). Comparing the theoretical value of 2.75 wt.-% carbon content to the measured values via GDOES it is obvious that the elemental quantification of this method is quite precise. Deviations from the theoretical value might origin from minor inaccuracies during the weighing of carbon containing slurry components (conductive additive and binder) and inaccuracy of the GDOES measurement. Looking at the 3 distributions of carbon mass fractions, all 3 differently manufactured electrodes show an accumulation of carbon close to the current collector. However in the bulk of the electrode distinct differences are visible: NMP-manufactured electrodes show the most homogeneous distribution while the DMSO- and TEP-manufactured ones show maxima of the carbon mass fraction in the middle area of the electrode and minima at both boundaries. The non-uniform carbon distribution of the TEP-processed electrode stands out in particular varying from 2.6% in the vicinity of the current collector up to 3.3% in the bulk of the electrode. In addition the TEP-processed electrode shows a sharp rise in carbon concentration in close distance to the surface.

Table 2
Mean capacity retention of cells with 3 mAh/cm^2 after 400 aging cycles at a current rate of 1 C.

	Capacity retention (C/10)	Capacity retention (1 C)
NMP	88.8%	75.4%
DMSO	85.7%	75.8%
TEP	86.6%	72.4%

The authors of [20] conclude that uneven carbon black distribution might lead to locally increased mechanical stress and result in contact loss between NCM particles and the carbon-binder domain, which could explain the herein observed differently pronounced aging behaviors of the cathodes. The most significant decrease in capacity during cyclization at 1 C is observed for the electrode prepared with TEP. This behavior is consistent with the results from [20], according to which a high carbon content far from and a low carbon content near to the current collector lead to more severe aging compared to a homogeneous distribution.

One possible reason for this uneven additive distribution is its migration during the drying process of electrodes for lithium-ion cells [21]. For future investigations this observation needs to be considered and might be an important clue to cope with the differently aging progresses.

Table 2 summarizes the cyclic aging results of Fig. 8 after 400 cycles. It is distinguished between capacity retention determined during the actual aging-cycles at 1 C and that determined via C/10 check-up-cycles, which are performed every 100 aging-cycles. For practical application the accessible capacity at high current (1 C) is more relevant than that at 1/10 C. It is notable that DMSO manufactured electrodes show a slightly higher capacity retention (at 1 C) after 400 cycles than the NMP reference. Keeping that but also the relatively high standard deviation in the last cycles in mind a conditional recommendation for DMSO as a candidate for replacing NMP can be made.

4. Conclusion

In this study we could show that less harmful substitutes for NMP as the state-of-the-art solvent for PVdF binder in the processing of cathodes for lithium-ion-cells do not have undesirable consequences for manufactured electrodes. With DMSO and TEP as solvents it is possible to realize similar viscosity of slurries at similar solid contents while maintaining coating properties. Furthermore neither in pulse

nor in rate or cycling tests of cells with a loading of 2 mAh/cm^2 serious deviations from NMP-processed electrodes were determined. Concluding from these tests it can be said that both alternatives behave in the same way and none should be preferred over the other.

Extensive cycle aging tests of cells with 3 mAh/cm^2 showed minor drawbacks of TEP regarding high current cycles (3 percentage points less capacity retention for TEP over 400 cycles compared to NMP). Considering 1 C cycles the DMSO manufactured electrodes show the same capacity retention like the NMP manufactured ones. Based on these results a conditional recommendation for DMSO as NMP replacing solvent can be made. Unevenly distributed conductive additive in both alternatively processed electrodes was identified via GDOES measurements and might serve as explanation for the slight deviations in capacity retention during cyclic aging. As an outlook to give an unconstrained recommendation the drying process as the most likely cause for the uneven carbon distribution should be optimized.

CRediT authorship contribution statement

Fabian Heim: Conceptualization, Investigation. **Frauke Langer:** Conceptualization, Investigation. **Anja Paulus:** Writing – review & editing. **Tina Kreher:** Writing – review & editing. **Peter Birke:** Supervision.

Declaration of competing interest

The authors declare the following financial interests/personal relationships which may be considered as potential competing interests: Fabian Heim reports financial support was provided by Mercedes-Benz Group AG .

Data availability

Data will be made available on request.

Acknowledgment

This work was supported by Mercedes-Benz Group AG .

References

[1] A. Kwade, W. Haselrieder, R. Leithoff, A. Modlinger, F. Dietrich, K. Droeder, Current status and challenges for automotive battery production technologies, Nature Energy 3 (4) (2018) 290–300.
[2] ANNEX XVII to reach, 2020, https://echa.europa.eu/documents/10162/e7598958-eae7-1661-0636-02778b427efc. Accessed: 2020-11-11.
[3] G. Schälicke, I. Landwehr, A. Dinter, K.-H. Pettinger, W. Haselrieder, A. Kwade, Solvent–free manufacturing of electrodes for lithium–Ion batteries via electrostatic coating, Energy Technol. 8 (2) (2020) 1900309.
[4] D. Bresser, D. Buchholz, A. Moretti, A. Varzi, S. Passerini, Alternative binders for sustainable electrochemical energy storage – the transition to aqueous electrode processing and bio-derived polymers, Energy Environ. Sci. 11 (11) (2018) 3096–3127.
[5] J.-H. Lee, S. Lee, U. Paik, Y.-M. Choi, Aqueous processing of natural graphite particulates for lithium-ion battery anodes and their electrochemical performance, J. Power Sources 147 (1–2) (2005) 249–255.
[6] N. Loeffler, G.-T. Kim, S. Passerini, C. Gutierrez, I. Cendoya, I. de Meatza, F. Alessandrini, G.B. Appetecchi, Performance and ageing robustness of graphite/NMC pouch prototypes manufactured through eco-friendly materials and processes, ChemSusChem 10 (18) (2017) 3581–3587.
[7] D.L. Wood, J.D. Quass, J. Li, S. Ahmed, D. Ventola, C. Daniel, Technical and economic analysis of solvent-based lithium-ion electrode drying with water and NMP, Drying Technol. 36 (2) (2018) 234–244.
[8] A. Bottino, G. Capannelli, S. Munari, A. Turturro, Solubility parameters of poly(vinylidene fluoride), J. Polym. Sci. B 26 (4) (1988) 785–794.
[9] J.E. Marshall, A. Zhenova, S. Roberts, T. Petchey, P. Zhu, C.E.J. Dancer, C.R. McElroy, E. Kendrick, V. Goodship, On the solubility and stability of polyvinylidene fluoride, Polymers 13 (9) (2021).
[10] M. Wang, X. Dong, I.C. Escobar, Y.-T. Cheng, Lithium ion battery electrodes made using dimethyl sulfoxide (DMSO)—A green solvent, ACS Sustain. Chem. Eng. 8 (30) (2020) 11046–11051.
[11] S.D. Hellring, M. Stewart, R.E. Daughenbaugh, Electrode slurry composition for lithium ion electrical storage devices, 2020.
[12] J. Chang, J. Zuo, L. Zhang, G.S. O'Brien, T.-S. Chung, Using green solvent, triethyl phosphate (TEP), to fabricate highly porous PVDF hollow fiber membranes for membrane distillation, J. Membr. Sci. 539 (2017) 295–304.
[13] V. Murray, D.S. Hall, J.R. Dahn, A guide to full coin cell making for academic researchers, J. Electrochem. Soc. 166 (2) (2019) A329–A333.
[14] S.J. An, J. Li, Z. Du, C. Daniel, D.L. Wood, Fast formation cycling for lithium ion batteries, J. Power Sources 342 (2017) 846–852.
[15] H. Li, J. Li, X. Ma, J.R. Dahn, Synthesis of single crystal LiNi 0.6 Mn 0.2 co 0.2 o 2 with enhanced electrochemical performance for lithium ion batteries, J. Electrochem. Soc. 165 (5) (2018) A1038–A1045.
[16] Y. Liu, J. Harlow, J. Dahn, Microstructural observations of "single crystal" positive electrode materials before and after long term cycling by cross-section scanning electron microscopy, J. Electrochem. Soc. 167 (2) (2020) 020512.
[17] U. Krewer, F. Röder, E. Harinath, R.D. Braatz, B. Bedürftig, R. Findeisen, Review—Dynamic models of li-ion batteries for diagnosis and operation: A review and perspective, J. Electrochem. Soc. 165 (16) (2018) A3656–A3673.
[18] W. Haselrieder, S. Ivanov, D.K. Christen, H. Bockholt, A. Kwade, Impact of the calendering process on the interfacial structure and the related electrochemical performance of secondary lithium-ion batteries, ECS Trans. 50 (26) (2013) 59–70.
[19] R. Morasch, J. Keilhofer, H.A. Gasteiger, B. Suthar, Methods—Understanding porous electrode impedance and the implications for the impedance analysis of Li-ion battery electrodes, J. Electrochem. Soc. 168 (8) (2021) 080519.
[20] S. Yari, H. Hamed, J. D'Haen, M.K. van Bael, F.U. Renner, Hardy, M. Safari, Constructive versus destructive heterogeneity in porous electrodes of lithium-ion batteries, ACS Appl. Energy Mater. 3 (12) (2020) 11820–11829.
[21] T. Lombardo, A.C. Ngandjong, A. Belhcen, A.A. Franco, Carbon-binder migration: A three-dimensional drying model for lithium-ion battery electrodes, Energy Storage Mater. 43 (2021) 337–347.